



King's Research Portal

DOI:

[10.1242/jcs.223974](https://doi.org/10.1242/jcs.223974)

Document Version

Peer reviewed version

[Link to publication record in King's Research Portal](#)

Citation for published version (APA):

Brayford, S., Kenny, F. N., Hiratsuka, T., Serna Morales, E., Yolland, L., Luchici, A., & Stramer, B. M. (2019). Heterotypic contact inhibition of locomotion can drive cell sorting between epithelial and mesenchymal cell populations. *Journal of Cell Science*, 132(11), [jcs223974]. <https://doi.org/10.1242/jcs.223974>

Citing this paper

Please note that where the full-text provided on King's Research Portal is the Author Accepted Manuscript or Post-Print version this may differ from the final Published version. If citing, it is advised that you check and use the publisher's definitive version for pagination, volume/issue, and date of publication details. And where the final published version is provided on the Research Portal, if citing you are again advised to check the publisher's website for any subsequent corrections.

General rights

Copyright and moral rights for the publications made accessible in the Research Portal are retained by the authors and/or other copyright owners and it is a condition of accessing publications that users recognize and abide by the legal requirements associated with these rights.

- Users may download and print one copy of any publication from the Research Portal for the purpose of private study or research.
- You may not further distribute the material or use it for any profit-making activity or commercial gain
- You may freely distribute the URL identifying the publication in the Research Portal

Take down policy

If you believe that this document breaches copyright please contact librarypure@kcl.ac.uk providing details, and we will remove access to the work immediately and investigate your claim.

Heterotypic contact inhibition of locomotion can drive cell sorting between epithelial and mesenchymal cell populations

Simon Brayford¹, Fiona N. Kenny¹, Toru Hiratsuka², Eduardo Serna-Morales¹, Lawrence Yolland¹, Andrei Luchici³, and Brian M. Stramer^{1*}

¹ Randall Centre for Cell and Molecular Biophysics, King's College London, SE1 1UL, London, United Kingdom

² Centre for Stem Cells and Regenerative Medicine, King's College London, SE1 9RT, London, United Kingdom

³ Dacian Consulting, 84 Brookwood Road, SW18 5BY, London, United Kingdom

* Correspondence: brian.m.stramer@kcl.ac.uk

ABSTRACT

1 Interactions between different cell-types can induce distinct contact inhibition of
2 locomotion (CIL) responses that are hypothesised to control population-wide
3 behaviours during embryogenesis. However, our understanding of the signals that
4 lead to cell-type specific repulsion and the precise capacity of heterotypic CIL
5 responses to drive emergent behaviours is lacking. Using a new model of heterotypic
6 CIL, we show that fibrosarcoma cells, but not fibroblasts, are actively repelled by
7 epithelial cells in culture. We show that knocking down EphB2 or ERK in fibrosarcoma
8 cells specifically leads to disruption of the repulsion phase of CIL in response to
9 interactions with epithelial cells. We also examine the population-wide effects when
10 these various cell combinations are allowed to interact in culture. Unlike fibroblasts,
11 fibrosarcoma cells completely segregate from epithelial cells and inhibiting their
12 distinct CIL response by knocking down EphB2 or ERK also disrupts this emergent
13 sorting behaviour. These data suggest that heterotypic CIL responses, in conjunction
14 with processes such as differential adhesion, may aid the sorting of cell populations.
15

16 INTRODUCTION

17 Contact inhibition of locomotion (CIL) is a process whereby a cell ceases
18 motility or changes trajectory upon collision with another cell. The response can occur
19 between cells of the same type (homotypic) or between different types (heterotypic)
20 leading to distinct dynamics depending on the cell-type and the receptors expressed
21 on their surface (Stramer and Mayor, 2016).

22 Our understanding of the functional significance of CIL for animal physiology is
23 only beginning to be elucidated. Differential homotypic and heterotypic CIL dynamics
24 have recently been shown to play a role in animal development (Theveneau et al.,
25 2013) and a loss of heterotypic CIL is hypothesised to play a role in cancer metastasis
26 (Abercrombie, 1979), yet the signals behind these responses are only starting to
27 emerge. In this study, through screening cell-types for distinct CIL behaviours we
28 report that fibrosarcoma cells, rather than losing their heterotypic CIL response after
29 contact with epithelial cells as previously predicted (Abercrombie, 1979), are actively
30 repelled via an Eph/ERK signalling cascade, highlighting that not all cancer cells are
31 necessarily CIL deficient. Interestingly, when fibrosarcoma and epithelial cells are
32 allowed to mix in culture, the heterotypic repulsion between them leads to sorting and
33 segregation of the populations. Recent work suggested that differential adhesion, the
34 predominant mechanism hypothesised to drive cell sorting, is inadequate in predicting
35 the segregation of mesenchymal populations (Pawlizak et al., 2015, Tambe and
36 Fredberg, 2015) and our data suggest that CIL may be an additional mechanism
37 behind this important developmental phenomenon.

38

39 RESULTS AND DISCUSSION

40 **Fibroblasts and fibrosarcoma cells exhibit distinct responses upon collision** 41 **with epithelial cells**

42 To study heterotypic cell-cell collisions, we used a confrontation assay whereby
43 two different cell populations were allowed to migrate and collide. Following a screen
44 of different epithelial versus mesenchymal cell-types, an unexpected phenomenon
45 was revealed. When migrating epithelial cells (HaCaT) encountered migrating
46 fibroblasts (NIH3T3), both populations ceased their forward motion, forming a sharp
47 border (Fig. 1A and Movie 1). In contrast, fibrosarcoma cells (HT1080) seemed to
48 undergo repulsion following collision with epithelial cells (Fig. 1A,B and Movie 1).
49 Interestingly, this repulsive response was not observed with melanoma cell-lines (Fig.

50 S1A,B and Movie 2), suggesting that fibrosarcoma cells may have an enhanced
51 heterotypic CIL response.

52 When no colliding partner was encountered, HaCaT cells migrated with a
53 constantly increasing speed (Fig. 1C), which was also observed following their
54 collision with HT1080 cells (Fig. 1D), suggesting that epithelial migration was
55 unaffected by collision with the HT1080 population. In contrast, HaCaT migration was
56 severely reduced following collision with fibroblasts (Fig. 1D). The repulsion of
57 fibrosarcoma cells was further analysed using particle image velocimetry, which
58 revealed a population-wide increase in epithelial cell speed following collision with
59 fibrosarcoma cells (Fig. 1E and Movie 3) showing that fibrosarcoma cells have a
60 distinct response to epithelial cells.

61

62 **Fibrosarcoma cells undergo active repulsion from epithelial cells**

63 To determine whether fibrosarcoma cell repulsion by epithelial cells was an
64 active process, we examined individual cell collisions (Movie 4). Analysis of
65 acceleration changes before and after collisions revealed that when fibrosarcoma cells
66 collided with epithelial cells there was a rapid, rearward acceleration (Fig. 2A)
67 suggesting a sudden change in motion. This response was similar to previously
68 reported collisions between *Drosophila* macrophages, which also undergo a classical
69 CIL response involving active repulsion (Davis et al., 2012, Davis et al., 2015). The
70 backward acceleration of fibrosarcoma cells was accompanied by a shift in the
71 direction of their velocities before, during, and after the collision as fibrosarcoma cells
72 were repelled from epithelial cells (Fig. 2B). In contrast, repulsion was not observed
73 when fibroblasts collided with epithelial cells, nor during homotypic fibrosarcoma
74 collisions, where cells continued to migrate toward the colliding partner after collision
75 (Fig. 2A and B). Plotting the distance from collision over time revealed that heterotypic
76 collisions led to fibrosarcoma cells slowing before migrating away from epithelial cells,
77 in contrast to homotypic collisions, which led to their continued forward motion (Fig.
78 2C). These data highlight that fibrosarcoma cells show distinct CIL dynamics involving
79 active repulsion in response to collision with epithelial cells.

80

81 **ERK activation downstream of EphB2 induces heterotypic repulsion of** 82 **fibrosarcoma cells**

83 There is much evidence for Eph receptors playing a role in epithelial cell

84 repulsion and cell segregation (Porazinski et al., 2016, Poliakov et al., 2008).
85 However, less is known about whether ephrin signalling may control the repulsion and
86 segregation of mesenchymal cell populations. HT1080 fibrosarcoma cells express the
87 ephrin receptor EphB2 (Fig. S2A), knockdown of which abolished the backward
88 acceleration upon collision with epithelial cells (Fig. 2A). This led to a random
89 distribution of cell velocities after collision (Fig. 2B) suggesting that cells were
90 randomly migrating away from epithelial cells rather than being actively repelled.
91 Similarly, plotting the distance from collision over time revealed that EphB2
92 knockdown in fibrosarcoma cells slowed their separation from epithelial cells, further
93 showing that the repulsion phase of CIL was disrupted (Fig. 2D). We also tested the
94 effect of knocking down EphB2 in the confrontation assay and found that indeed,
95 collective repulsion of fibrosarcoma cells following collision with a monolayer of
96 epithelial cells was also impaired (Fig. S2C,D).

97 One signalling pathway previously reported to be controlled by Eph receptor
98 activation is the ERK pathway. However, there is conflicting evidence for ERK
99 signalling specifically downstream of Eph receptor activation, with some reports
100 suggesting inhibition (Miao et al., 2003, Elowe et al., 2001) and others reporting an
101 increase following Eph receptor stimulation (Pratt and Kinch, 2002, Vindis et al., 2003,
102 Kandouz et al., 2010). We found that knockdown of ERK1/2 in fibrosarcoma cells
103 phenocopied EphB2 knockdown both in single-cell collisions (Fig. 2A,B,D) and in
104 confrontation assays (Fig. S2C,D). To confirm that these effects were related to
105 collisions and not general migration defects we examined non-colliding fibrosarcoma
106 cells and found no significant difference in either speed (Fig. S2E) or persistence (Fig.
107 S2F) following EphB2 or ERK knockdown.

108 We also examined the temporal relationship between protrusion/retraction
109 events surrounding collisions. We found that both EphB2 and ERK1/2 knockdown in
110 fibrosarcoma cells led to a delay in leading-edge retraction following contact with
111 epithelial cells (Fig. 2E). This was accompanied by a disruption to the
112 protrusion/retraction sequence where, unlike control cells which retracted their
113 leading-edge before forming a new protrusion, both EphB2 and ERK knockdown cells
114 often formed a new protrusion prior to leading-edge retraction (Fig. 2F) suggesting a
115 loss of coordinated retraction and repolarisation of lamellae after collision.
116 Interestingly, ERK was recently shown to regulate various cytoskeletal and migratory
117 behaviours (Yang et al., 2018, Mendoza et al., 2011, Aoki et al., 2017) and we

118 hypothesise that ERK is a good candidate to modulate distinct CIL dynamics.

119 To examine ERK activity during heterotypic interactions, we used western
120 blotting to probe lysates from co-cultures for pERK and found that pERK was elevated
121 among epithelial-fibrosarcoma co-cultures compared with either of these cell-types
122 individually (Fig. 3A) suggesting that ERK activity increased when these cell-types
123 interacted. We also found that EphB2 knockdown in fibrosarcoma cells, whilst not
124 affecting total ERK levels (Fig. 3B), resulted in a significant decrease in pERK in
125 epithelial-fibrosarcoma co-cultures (Fig. 3C), suggesting that ERK activation is
126 downstream of EphB2 in the fibrosarcoma population.

127 To analyse ERK activation dynamics during individual cell-cell interactions, we
128 used a FRET biosensor which has previously been demonstrated to report ERK
129 activity in living cells (Komatsu et al., 2011). Using cells expressing the biosensor, we
130 found in confrontation assays that ERK activity increased in fibrosarcoma cells at the
131 migrating front after colliding with epithelial cells (Fig. 3D,E and Movie 5), but not in
132 fibroblasts after colliding with epithelial cells (Figs. 3F and S3). We also examined co-
133 cultures of fibrosarcoma and epithelial cells and found higher ERK activity among
134 fibrosarcoma cells in the presence of epithelial cells compared to fibrosarcoma cells
135 alone (Fig. 3G). Finally, we found that cells in the mixed group had a higher fluctuation
136 in their ERK activity over time by measuring variance in ERK activity compared to
137 fibrosarcoma only (Fig. 3H), and we hypothesise that this was due to fibrosarcoma
138 cells constantly undergoing heterotypic collisions throughout the course of the assay.
139 Taken together, these data suggest that ERK signalling acts downstream of EphB2
140 and is involved in the repulsion of fibrosarcoma cells upon their contact with epithelial
141 cells.

142

143 **Fibrosarcoma and epithelial cell populations sort in culture through CIL** 144 **interactions**

145 To examine how heterotypic CIL affects population dynamics, we generated
146 time-lapse movies of co-cultures, and found that epithelial cells and fibroblasts formed
147 a homogenous, interspersed population, in contrast to epithelial and fibrosarcoma
148 cells, which immediately began to sort from one another (Fig. 4A and Movie 6). In
149 addition, automated tracking of the mesenchymal cells in these movies revealed a
150 streaming-type behaviour specifically among fibrosarcoma cells (Fig. 4B and Movie

151 6), highlighting this population's coordinated segregation from epithelial cells over
152 time.

153 To examine whether the specific repulsive CIL dynamics of fibrosarcoma cells
154 in response to epithelial cells was driving their segregation we inhibited Eph or ERK
155 signalling in the fibrosarcoma population. Indeed, knockdown of EphB2 or ERK1/2 in
156 fibrosarcoma cells resulted in a disruption to their segregation from epithelial cells (Fig.
157 4C,D). Similarly, treatment with U0126 also resulted in disruption to the segregation
158 between fibrosarcoma and epithelial cells (Fig. S4A-C). These data suggest that
159 segregation of fibrosarcoma from epithelial cells is driven by active repulsion between
160 these two populations.

161 We also investigated the phenomenon of cell-sorting over a longer period to
162 examine the final patterns of the populations (Fig. 4E). Alone, epithelial cells grew in
163 clusters that eventually merged to form large colonies. However, the presence of
164 fibroblasts resulted in much smaller clusters as the two cell populations reached
165 equilibrium. In contrast, when grown together with fibrosarcoma cells, which
166 proliferate at a similar rate to fibroblasts (Fig. S4D), epithelial cells formed large
167 colonies unimpeded by the presence of fibrosarcoma cells (Fig. 4E). Furthermore,
168 epithelial cell proliferation was specifically reduced in the presence of fibroblasts (Fig.
169 4F) suggesting they may undergo contact inhibition of proliferation in the absence of
170 a repulsive heterotypic CIL response. Finally, we measured the size of individual
171 epithelial cells and found that those in contact with fibroblasts failed to spread
172 compared with those in contact with fibrosarcoma cells (Figs 4G and S4E). These
173 data suggest that the repulsion of fibrosarcoma cells allows the epithelial cells to
174 spread which may enable their proliferation, similar to other epithelial cell-types
175 (Gumbiner and Kim, 2014, Aragona et al., 2013).

176 The differential adhesion hypothesis (DAH) states that two different cell-types
177 can segregate simply by taking into account their differential adhesion and surface
178 tension (Foty and Steinberg, 2013). This has been the predominant model to explain
179 cell-sorting and assumes that cells segregate in a liquid-like phase separation. The
180 problem with this concept is that groups of cells do not behave like perfect liquids; cell
181 clusters can quickly go from a fluid-like to a solid-like state as cell density increases
182 in a process termed 'jamming', which leads to cells rapidly slowing their motion (Sadati
183 et al., 2013). Furthermore, the DAH has recently been found inadequate in predicting
184 the sorting of mesenchymal cells (Pawlizak et al., 2015, Tambe and Fredberg, 2015).

185 Here we show that a mesenchymal cell-type can rapidly segregate from an
186 epithelial population. Differential adhesion is still playing a role in this case due to the
187 high surface-tension of the epithelial population and the near-non-existent mutual
188 adhesion of the fibrosarcoma cells, leading to the less cohesive cell (HT1080)
189 surrounding the more cohesive cell-type (HaCaT) as expected by DAH (Foty and
190 Steinberg, 2013). However, DAH is insufficient on its own, as inhibiting heterotypic
191 repulsion prevents sorting. We hypothesise that CIL between fibrosarcoma and
192 epithelial cells helps fluidise the population, allowing cells to sample their adhesive
193 landscape. Furthermore, there appears to be an aspect of fibrosarcoma CIL relieving
194 contact inhibition of proliferation of epithelial cells, allowing epithelial colonies to grow
195 and merge (Fig. S5). It is therefore possible that we are also highlighting an
196 unexplored connection between CIL and contact inhibition of proliferation despite
197 these processes being thought of as distinct behaviours (Stramer and Mayor, 2016).

198 It was previously hypothesised that one hallmark of cancer cells is a loss of CIL
199 in response to neighbouring cells, which may aid their metastatic spread. However,
200 here we reveal that not all cancer cells are deficient in heterotypic CIL; indeed,
201 fibrosarcoma cells show a robust repulsive CIL response after contact with epithelial
202 cells. One question is whether such a response is physiologically relevant. It is
203 possible that both positive and negative CIL behaviours of some cancer cells
204 observed *in vitro* may be related to an ontogenetic theory of cancer dissemination; it
205 was recently hypothesised that some cancers may spread through permissive
206 compartments that are defined embryologically (Hockel, 2012, Hockel, 2015) and it
207 will be interesting to determine whether differential CIL dynamics may be playing a
208 role in the compartmentalised spreading of metastatic cells *in vivo*.

209

MATERIALS AND METHODS

210

Cell culture

212 Cell-lines were a gift from Vicky Sanz-Moreno and Matthias Krause and were routinely
213 tested and found to be free from mycoplasma contamination. Cells were maintained
214 in DMEM (Sigma, St. Louis, MI cat# 6429) supplemented with 10 % FBS, at 37° C
215 and 5 % CO₂. For routine maintenance, cells were cultured in T75 plastic cell culture
216 flasks and split via trypsinisation approximately every 3 days or when approaching
217 confluence.

218 **Cell labelling**

219 CellTracker Green CMFDA and CellTracker Red CMTPX dyes (Invitrogen, Carlsbad,
220 CA) were used to differentially label cell-types in co-culture assays. Cells were
221 exposed to either dye at 1 μ M in serum-free medium for 30 mins at 37° C before being
222 washed once with PBS, trypsinised and re-suspended in complete medium.

223 **Imaging**

224 Movies and still images were acquired using an LSM 880 inverted confocal
225 microscope (Zeiss, Oberkochen, Germany). Cells were maintained at 37° C and 5 %
226 CO₂ for the duration of live imaging. Images were acquired using differential
227 interference contrast (DIC) imaging along with airyscan filter sets for 488 or 561 lasers
228 with either a 20X (NA 0.45) air objective (Zeiss).

229 **Confrontation assay**

230 2-well culture inserts (Ibidi, Germany) were placed into the centre of the well of a 24
231 well μ -Plate (Ibidi, Germany). Two different pre-labelled cell-types were seeded into
232 opposite chambers at a density of 1 x 10⁵ cells / cm² and incubated overnight. The
233 culture insert was then removed and the well topped up with 1 mL culture medium
234 before live imaging of the resulting 500 μ m gap.

235 **Particle image velocimetry (PIV)**

236 Time-lapse images were manually segmented prior to analysis and pseudo-speckle
237 analysis was performed as described previously (Betz et al., 2009). The size of the
238 search image was chosen such that it spanned the maximum expected displacement
239 of the cells during the acquisition time. To cover the whole search image, a cross-
240 correlation coefficient was computed between source image and a sub-image of the
241 search image shifted by one pixel. Finally, a spatial convolution with a Gaussian kernel
242 and temporal convolution were used to interpolate the measured displacements to
243 cover all the pixels within the frame. The complete algorithm for this analysis, including
244 the filtering and interpolation was implemented in MATLAB (MathWorks[®], Natick, MA).

245 **Individual cell collisions and manual tracking**

246 Analysis of single-cell collisions was carried out by combining cells pre-labelled with
247 Cell-Tracker Dyes (Invitrogen) at low density, plating sparsely and allowing to adhere
248 4 h before imaging every 1 min. For the kinematics analysis, a collision was defined
249 as the timepoint the cell in question contacts any part of the colliding partner. The cell
250 nucleus, which could be identified from DIC movies was manually tracked using the
251 mTrackJ plugin for ImageJ (NIH) to calculate the x,y coordinates of the cell at all time-

252 points.

253 **Kinematics analysis**

254 Kinematics analysis of the velocity and acceleration of cells was calculated as
255 previously described (Dunn and Paddock, 1982, Davis et al., 2015). In order to assess
256 the statistical significance of the direction of cells after collision, a binomial test with a
257 probability of success of 95% was performed on the cell velocity unit vectors every
258 five minutes from 5 min before to 20 min after collision. To assess the statistical
259 significance of acceleration, a one-sample t-test of the horizontal component of the
260 vectors was performed.

261 **Gene silencing by small interfering RNA (siRNA)**

262 HT1080 cells were plated onto 6-well plates at 2×10^5 cells / well and allowed to attach
263 overnight. Cells were transfected with pre-validated siRNA sequences to knockdown
264 human EphB2 (Sigma, cat. no. EHU060511) or human p44/42 MAPK (ERK1/2) (Cell
265 Signalling Technologies, Cat no. 6560). Unless otherwise stated in the figure legends,
266 AllStars Negative Control siRNA (Qiagen, Venlo, Netherlands) was used as a
267 negative control. siRNA was transfected using Lipofectamine RNAiMAX reagent
268 (Invitrogen, Carlsbad, CA) according to the manufacturer's instructions. Experiments
269 were carried out 48 h post-transfection.

270 **Western blotting and antibodies**

271 Total cellular proteins from individual cells or co-cultured populations were prepared
272 by rinsing cells with cold PBS and scraping with RIPA buffer (20 mM Tris pH 7.4, 150
273 mM sodium chloride, 1% (v/v) Nonidet P-40, 0.5% (w/v) sodium deoxycholate, 1 mM
274 EDTA, 0.1% (w/v) SDS) in the presence of protease and phosphatase inhibitor
275 cocktails (Roche Diagnostics, Indianapolis, IN). 20 μ g of protein per well was resolved
276 on 12.5% SDS-PAGE gels before electro-transfer to PVDF membranes. Following
277 blocking in 5% (w/v) BSA in TBST, immunoblotting was performed using anti-EphB2
278 (Cell Signalling Technology, Danvers, MA, cat. #83029), anti-GADPH (Millipore,
279 Burlington, MA, cat. #ABS16), anti-p44/42 MAPK (Cell Signalling #9102), anti-cofilin
280 (CST #5175) or anti-Phospho-p44/42 MAPK (Cell Signalling #9101) antibodies at 1 in
281 1000 dilution to detect EphB2, GAPDH, ERK1/2, cofilin and pERK1/2 (Thr202/Tyr204)
282 protein respectively. Membranes were then washed with TBST and incubated with
283 species appropriate HRP-conjugated IgG secondary antibodies (Dako, Agilent
284 Technologies, Santa Clara, CA) at 1 in 10,000. Chemiluminescence was measured
285 using ImageJ (NIH, Bethesda, MD) after applying Clarity™ Western ECL substrate

286 (BioRad, Hercules, CA).

287 **FRET biosensor plasmid and Lentiviral transduction**

288 The lentiviral plasmid of nucleus-localised FRET biosensor for ERK (EKAREV-NLS)
289 has been previously characterised (Komatsu et al., 2011) and was a kind gift from
290 Michiyuki Matsuda at Kyoto University, Japan. EKAREV-NLS ERK biosensor was
291 expressed in HT1080 cells by lentiviral transduction. EKAREV-ELS in replication-
292 defective, self-inactivating lentiviral pCSII vector was co-transfected with packaging
293 plasmid (pCAG-HIVgp) and VSV-G-/Rev-expressing plasmid (pCMV-VSVG-RSV-
294 Rev) into Lenti-X 293T cells (Clontech, Mountain View, CA). High-titre viral solution
295 was prepared and used for transduction into cells. NIH3T3 cells were transfected with
296 a pPBbsr-EKAREV-NLS plasmid encoding EKAREV-NLS in pPB piggyback
297 backbone using jetPRIME reagent (Polyplus Transfection SA, Illkirch, France)
298 following the manufacturer's instructions.

299 **FRET Imaging**

300 FRET images were obtained following methods previously reported (Aoki and
301 Matsuda, 2009). Cells were imaged with an LSM 880 inverted confocal microscope
302 (Zeiss, Oberkochen, Germany) using a 40X (NA 0.95) oil objective (Zeiss). Donor
303 fluorescence protein was excited with a 458 nm laser to obtain donor and FRET signal
304 by detection filters 483/32 and 542/27, respectively. ERK activity was determined by
305 ratiometry (FRET/CFP) as validated previously (Aoki and Matsuda, 2009, Komatsu et
306 al., 2011). Pseudocolour images of ERK activity (Fig. 3D) were shown in intensity
307 modulated display (IMD). Confrontation assay FRET measurements were taken 30
308 mins before or 30 mins after the frame at which cell-cell collision occurred.

309 **Short-term co-culture assays**

310 Cells were pre-labelled with either cell-tracker red or green, counted and combined in
311 1:1 suspension so that 5×10^4 of each cell-type was seeded per well in a 24-well
312 imaging μ -Plate (total of 1×10^5 cells / well). For Wild-Type assays, cells were allowed
313 6 h to adhere before being imaged overnight for a total of 22 h. For RNAi experiments,
314 cells were transfected with siRNA for 48 h before being differentially labelled,
315 combined allowed to mix for 24 h before fixation with 4% paraformaldehyde in PBS.
316 All nuclei were then labelled with DRAQ5 (Invitrogen) before coverslips were
317 mounted. Still Images were then acquired, and the green channel was used to create
318 a mask over the HT1080 cells' nuclei, leaving only the HaCaT cells' nuclei visible for
319 segmentation. Nearest neighbour distances were then calculated in ImageJ (NIH). For

320 U0126 MEK inhibition movies, cells were differentially labelled before being combined
321 and allowed to adhere for 6 h. U0126 (Sigma) was then added at a concentration of
322 20µM to inhibit MEK/ERK signalling alongside DMSO as vehicle control, and live
323 imaging was then commenced immediately for a total of 24 h. For quantitative
324 analysis, HaCaT cells at 6 h and 24 h were manually segmented and nearest-
325 neighbour distances were calculated in ImageJ (NIH).

326 **Automated cell tracking**

327 For automated tracking, the image channel corresponding to NIH3T3 or HT1080 cells
328 was thresholded in ImageJ so that individual cells could be detected as particles in
329 the TrackMate plugin and tracks generated for all cells.

330 **Long-term co-culture assay**

331 HaCaT cells were pelleted by centrifugation and re-suspended in CellTrace™ CFSE
332 (Invitrogen) at a working concentration of 5 µM in PBS and incubated for 20 minutes
333 at 37°C. Cells were again pelleted and re-suspended in fresh culture medium to a
334 density of 2×10^4 cells / mL and incubated for 10 minutes to allow the CFSE reagent
335 to undergo acetate hydrolysis. This suspension was then combined with either DMEM
336 (control), an NIH3T3 cell suspension (unlabelled) or HT1080 cell suspension
337 (unlabelled) and added to a 24-well plate for a total of 20,000 cells per well and
338 incubated for 4 days, fixing with 4% paraformaldehyde every 24 h and mounting
339 coverslips with ProlongGold (Invitrogen). Coverslips were then imaged with a 20x air
340 objective for further analysis using ImageJ (NIH).

341 **Proliferation assay**

342 NIH3T3 and HT1080 cells were seeded in a 96-well plate at 1000 cells per well and
343 incubated for 4 h. Growth medium was then carefully removed and 1X CyQUANT®
344 NF (Invitrogen) dye reagent was added. Cells were then incubated at 37°C for 1 h.
345 This incubation period is required for equilibration of dye–DNA binding, resulting in a
346 stable fluorescence endpoint. The fluorescence intensity of each sample was then
347 imaged every 24 h using a fluorescence microplate reader with excitation at ~485 nm
348 and emission detection at ~530 nm. Fresh growth medium was added every 48 h. Cell
349 numbers at each time-point were determined using a standard curve as per the
350 manufacturer's instructions.

351 **Statistical analyses**

352 Statistical analyses are described in each figure legend.

353

REFERENCES

- 354 ABERCROMBIE, M. 1979. Contact inhibition and malignancy. *Nature*, 281, 259-62.
- 355 AOKI, K., KONDO, Y., NAOKI, H., HIRATSUKA, T., ITOH, R. E. & MATSUDA, M.
- 356 2017. Propagating Wave of ERK Activation Orients Collective Cell Migration.
- 357 *Dev Cell*, 43, 305-317 e5.
- 358 AOKI, K. & MATSUDA, M. 2009. Visualization of small GTPase activity with
- 359 fluorescence resonance energy transfer-based biosensors. *Nat Protoc*, 4,
- 360 1623-31.
- 361 ARAGONA, M., PANCIERA, T., MANFRIN, A., GIULITTI, S., MICHIELIN, F.,
- 362 ELVASSORE, N., DUPONT, S. & PICCOLO, S. 2013. A mechanical
- 363 checkpoint controls multicellular growth through YAP/TAZ regulation by actin-
- 364 processing factors. *Cell*, 154, 1047-1059.
- 365 BETZ, T., KOCH, D., LIM, D. & KAS, J. A. 2009. Stochastic actin polymerization and
- 366 steady retrograde flow determine growth cone advancement. *Biophys J*, 96,
- 367 5130-8.
- 368 DAVIS, J. R., HUANG, C. Y., ZANET, J., HARRISON, S., ROSTEN, E., COX, S.,
- 369 SOONG, D. Y., DUNN, G. A. & STRAMER, B. M. 2012. Emergence of
- 370 embryonic pattern through contact inhibition of locomotion. *Development*, 139,
- 371 4555-60.
- 372 DAVIS, J. R., LUCHICI, A., MOSIS, F., THACKERY, J., SALAZAR, J. A., MAO, Y.,
- 373 DUNN, G. A., BETZ, T., MIODOWNIK, M. & STRAMER, B. M. 2015. Inter-
- 374 cellular forces orchestrate contact inhibition of locomotion. *Cell*, 161, 361-73.
- 375 DUNN, G. A. & PADDOCK, S. W. 1982. Analysing the motile behaviour of cells: a
- 376 general approach with special reference to pairs of cells in collision. *Philos*
- 377 *Trans R Soc Lond B Biol Sci*, 299, 147-57.
- 378 ELOWE, S., HOLLAND, S. J., KULKARNI, S. & PAWSON, T. 2001. Downregulation
- 379 of the Ras-mitogen-activated protein kinase pathway by the EphB2 receptor
- 380 tyrosine kinase is required for ephrin-induced neurite retraction. *Mol Cell Biol*,
- 381 21, 7429-41.
- 382 FOTY, R. A. & STEINBERG, M. S. 2013. Differential adhesion in model systems.
- 383 *Wiley Interdiscip Rev Dev Biol*, 2, 631-45.
- 384 GUMBINER, B. M. & KIM, N. G. 2014. The Hippo-YAP signaling pathway and
- 385 contact inhibition of growth. *J Cell Sci*, 127, 709-17.
- 386 HOCKEL, M. 2012. Cancer permeates locally within ontogenetic compartments:
- 387 clinical evidence and implications for cancer surgery. *Future Oncol*, 8, 29-36.
- 388 HOCKEL, M. 2015. Morphogenetic fields of embryonic development in locoregional
- 389 cancer spread. *Lancet Oncol*, 16, e148-51.
- 390 KANDOUZ, M., HAIDARA, K., ZHAO, J., BRISSON, M. L. & BATIST, G. 2010. The
- 391 EphB2 tumor suppressor induces autophagic cell death via concomitant
- 392 activation of the ERK1/2 and PI3K pathways. *Cell Cycle*, 9, 398-407.
- 393 KOMATSU, N., AOKI, K., YAMADA, M., YUKINAGA, H., FUJITA, Y., KAMIOKA, Y.
- 394 & MATSUDA, M. 2011. Development of an optimized backbone of FRET
- 395 biosensors for kinases and GTPases. *Mol Biol Cell*, 22, 4647-56.
- 396 MENDOZA, M. C., ER, E. E., ZHANG, W., BALLIF, B. A., ELLIOTT, H. L.,
- 397 DANUSER, G. & BLENIS, J. 2011. ERK-MAPK drives lamellipodia protrusion
- 398 by activating the WAVE2 regulatory complex. *Mol Cell*, 41, 661-71.
- 399 MIAO, H., NICKEL, C. H., CANTLEY, L. G., BRUGGEMAN, L. A., BENNARDO, L.
- 400 N. & WANG, B. 2003. EphA kinase activation regulates HGF-induced
- 401 epithelial branching morphogenesis. *J Cell Biol*, 162, 1281-92.

402 PAWLIZAK, S., FRITSCH, A. W., GROSSER, S., AHRENS, D., THALHEIM, T.,
403 RIEDEL, S., KIEßLING, T. R., OSWALD, L., ZINK, M., MANNING, M. L. &
404 KÄS, J. A. 2015. Testing the differential adhesion hypothesis across the
405 epithelial–mesenchymal transition. *New J Phys*, 17, 083049.
406 POLIAKOV, A., COTRINA, M. L., PASINI, A. & WILKINSON, D. G. 2008. Regulation
407 of EphB2 activation and cell repulsion by feedback control of the MAPK
408 pathway. *J Cell Biol*, 183, 933-47.
409 PORAZINSKI, S., DE NAVASCUES, J., YAKO, Y., HILL, W., JONES, M. R.,
410 MADDISON, R., FUJITA, Y. & HOGAN, C. 2016. EphA2 Drives the
411 Segregation of Ras-Transformed Epithelial Cells from Normal Neighbors. *Curr*
412 *Biol*, 26, 3220-3229.
413 PRATT, R. L. & KINCH, M. S. 2002. Activation of the EphA2 tyrosine kinase
414 stimulates the MAP/ERK kinase signaling cascade. *Oncogene*, 21, 7690-9.
415 SADATI, M., TAHERI QAZVINI, N., KRISHNAN, R., PARK, C. Y. & FREDBERG, J.
416 J. 2013. Collective migration and cell jamming. *Differentiation*, 86, 121-5.
417 STRAMER, B. & MAYOR, R. 2016. Mechanisms and in vivo functions of contact
418 inhibition of locomotion. *Nat Rev Mol Cell Biol*.
419 TAMBE, D. T. & FREDBERG, J. J. 2015. And I hope you like jamming too. *New J*
420 *Phys*, 17, 091001.
421 THEVENEAU, E., STEVENTON, B., SCARPA, E., GARCIA, S., TREPAT, X.,
422 STREIT, A. & MAYOR, R. 2013. Chase-and-run between adjacent cell
423 populations promotes directional collective migration. *Nat Cell Biol*, 15, 763-
424 72.
425 VINDIS, C., CERRETTI, D. P., DANIEL, T. O. & HUYNH-DO, U. 2003. EphB1
426 recruits c-Src and p52Shc to activate MAPK/ERK and promote chemotaxis. *J*
427 *Cell Biol*, 162, 661-71.
428 YANG, J. M., BHATTACHARYA, S., WEST-FOYLE, H., HUNG, C. F., WU, T. C.,
429 IGLESIAS, P. A. & HUANG, C. H. 2018. Integrating chemical and mechanical
430 signals through dynamic coupling between cellular protrusions and pulsed
431 ERK activation. *Nat Commun*, 9, 4673.

Funding

This project has received funding from the European Research Council (ERC) under the European Union's Horizon 2020 research and innovation program grant agreement No. 681808. T.H. has received funding from the European Union's Horizon 2020 research and innovation program under the Marie Skłodowska-Curie grant agreement No. 704587. F.N.K. and B.M.S. are funded by a Wellcome Trust Investigator Award, grant number WT107859/Z/15/Z. Deposited in PMC for release....

Figure Legends

432 **Fig. 1. Fibroblasts and fibrosarcoma cells exhibit distinct responses upon**
433 **collision with epithelial cells**

434 (A) Confrontation assay between epithelial cells (HaCaT, green) and fibroblasts
435 (NIH3T3, magenta) or fibrosarcoma cells (HT1080, magenta). Red line indicates
436 collision-point. Scale bars = 100 μ m.

437 (B) HaCaT displacement 24 h after colliding with NIH3T3 or HT1080 cells (n = 3, error
438 bars = SEM, ***P < 0.001).

439 (C) Leading-edge speed of migrating HaCaT cells when no other cell population is
440 encountered (n = 3, error bars = SEM).

441 (D) Leading-edge speed of migrating HaCaT cells involving collision with either
442 NIH3T3 or HT1080 cell populations. Dotted line indicates collision-point (n = 3,
443 error bars = SEM).

444 (E) PIV analysis of the HaCaT and HT1080 interaction in 'A' showing global increase
445 in HaCaT speed despite collision with HT1080 cells. Blue-red represents a shift
446 from low to high velocity.

447

448 **Fig. 2. Fibrosarcoma cells undergo active repulsion upon collision with**
449 **epithelial cells which is perturbed by EphB2 or ERK1/2 knockdown**

450 (A) Vectors depicting acceleration changes upon collision (time = 0 min) normalised
451 to the position of the colliding partner (large arrow). A significant rearward
452 acceleration (**P < 0.01, non-parametric Wilcoxon signed-rank test) is only
453 observed in HT1080 vs HaCaT collision (n \geq 6 collisions).

454 (B) Vectors depicting velocity of colliding cells before, at time of, and after collision
455 normalised to the position of the colliding partner (large arrow). A significant post-
456 collision rearward velocity away from the colliding partner (*P < 0.05, non-
457 parametric Wilcoxon signed-rank test) is only observed in HT1080 vs HaCaT (n \geq
458 6 collisions).

459 (C) Cell distance from colliding partner during heterotypic and homotypic collisions
460 between HT1080, NIH3T3, and HaCaT cells. Following collision (dotted line), only
461 HT1080 and HaCaT cells rapidly separate (n \geq 6 collisions, error bars = SEM).

- 462 (D) Cell distance from colliding partner during heterotypic HaCaT-HT1080 collisions
463 comparing non-transfected (HaCaT vs HT1080 from 'C') with EphB2 or ERK1/2
464 knockdown (HT1080) ($n \geq 6$ collisions, error bars = SEM).
- 465 (E) Time taken for HT1080 cells to retract their leading-edge following contact with
466 HaCaT cells ($n \geq 7$ collisions per condition, line = mean, error bars \pm SD, * $P < 0.05$,
467 ** $P < 0.01$, Student's t-test).
- 468 (F) Time between leading-edge retraction and formation of a protrusion in HT1080
469 cells following contact with HaCaT cells. Negative values indicate that formation of
470 the new protrusion occurred *before* leading-edge retraction ($n \geq 7$ collisions, line =
471 mean, error bars \pm SD, ** $P < 0.01$, **** $P < 0.0001$, Student's t-test).

472

473 **Fig. 3. ERK activation is elevated in collisions between epithelial and**
474 **fibrosarcoma cells**

- 475 (A) Western blot reveals pERK was highest during co-culture of HaCaT and HT1080
476 cells. ($n = 3$, error bars = SEM).
- 477 (B) Western blot and quantification showing total ERK was unaffected by EphB2
478 knockdown in HT1080 cells compared with non-transfected control. ($n = 3$, error
479 bars = SEM, ns = not statistically significant, Student's t-test).
- 480 (C) Western blot and quantification showing pERK was significantly reduced in the
481 co-culture after EphB2 knockdown in HT1080 cells compared with non-transfected
482 control. ($n = 3$, error bars = SEM, ** $P < 0.01$, Student's t-test).
- 483 (D) Confrontation assay between HaCaT cells (unlabelled) and HT1080 cells
484 expressing the ERK FRET-biosensor. Scale bar = 50 μm .
- 485 (E) ERK activity in the leading row of HT1080 cells in the confrontation assay before
486 collision, after collision and in rear cells after collision. ($n = 29$ cells per condition,
487 boxplots represent range, median and quartiles, * $P < 0.05$, *** $P < 0.001$ Mann-
488 Whitney test).
- 489 (F) ERK activity in the leading row of NIH3T3 cells in the confrontation assay before
490 and after collision ($n = 23$ cells per condition, boxplots represent range, median
491 and quartiles, ns = not statistically significant, Mann-Whitney test).
- 492 (G) ERK activity from four representative tracks of HT1080 cells cultured alone (blue)
493 or co-cultured with HaCaT cells (red).
- 494 (H) Fluctuation of ERK activity as measured by variance in randomly selected tracks

495 of HT1080 cells cultured alone or co-cultured with HaCaT cells. (n = 15 tracks, line
496 = mean, error bars \pm SD, ***P < 0.001, Mann-Whitney test).

497

498 **Fig. 4. Fibrosarcoma cells sort from epithelial cells in culture, a behaviour which**
499 **is disrupted by EphB2 or ERK1/2 knockdown**

500 (A) Screenshots from movies of co-cultures of epithelial cells (HaCaT, green) with
501 either fibroblasts (NIH3T3, magenta) or fibrosarcoma cells (HT1080, magenta).
502 Scale bar = 100 μ m.

503 (B) Tracks of NIH3T3 or HT1080 cells throughout the movies in 'A'.

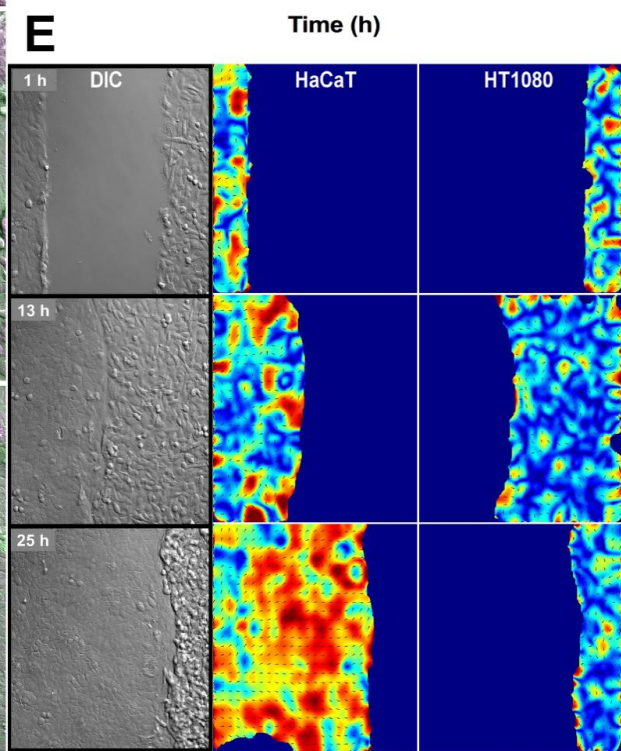
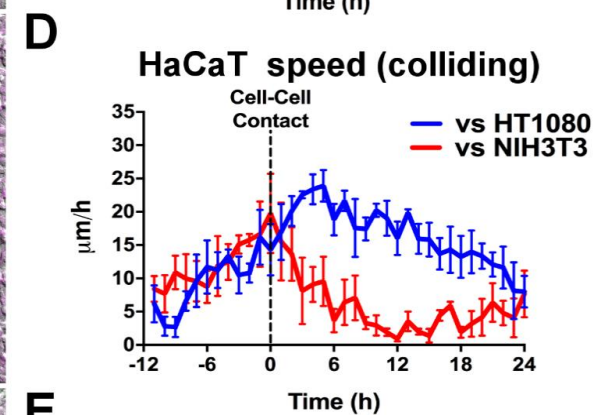
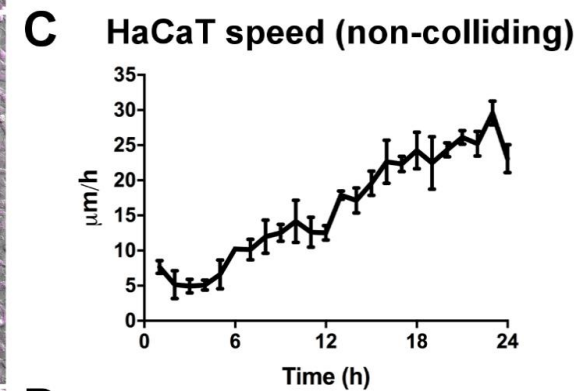
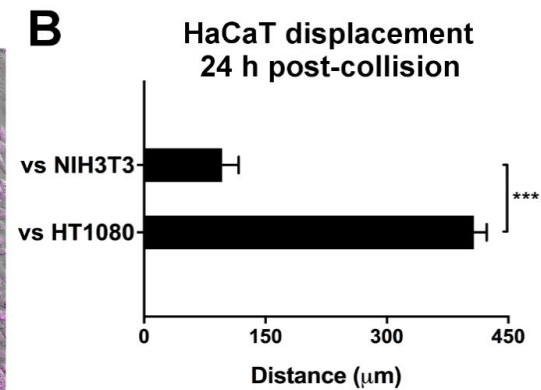
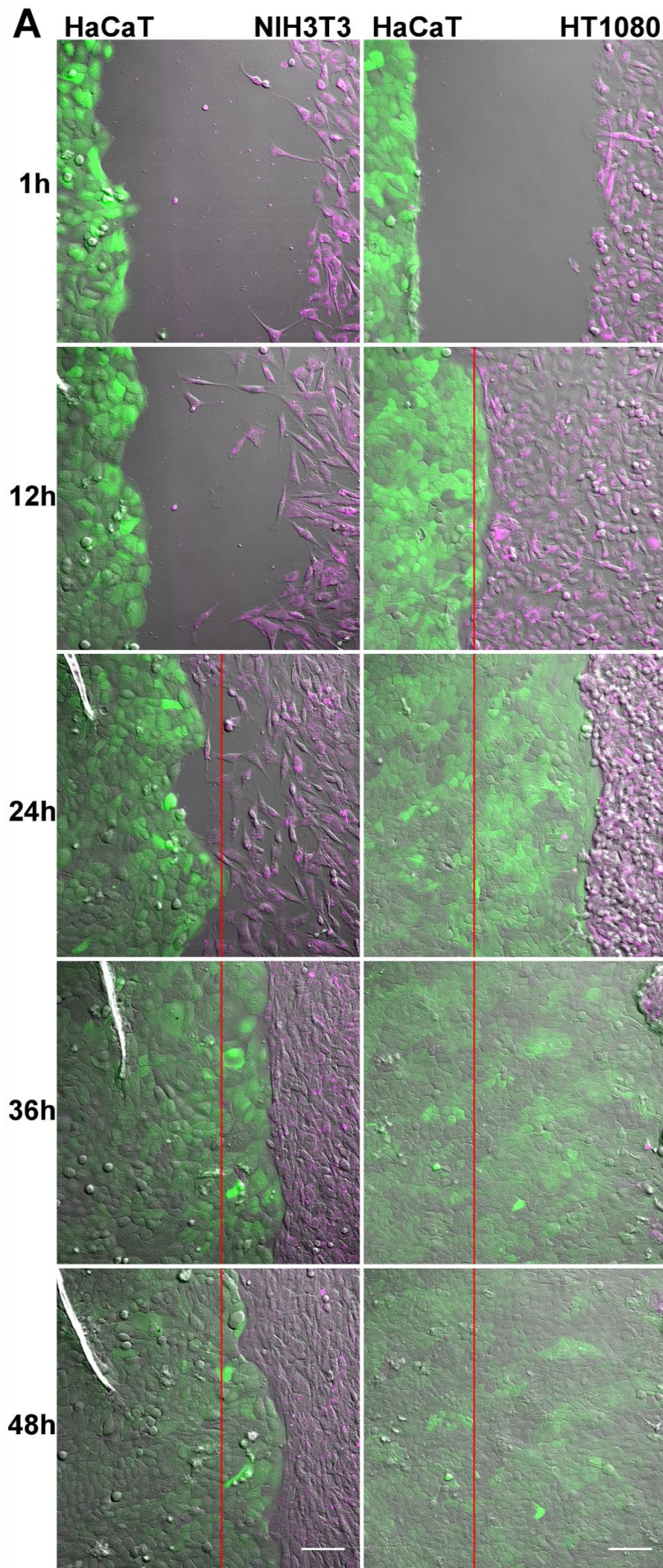
504 (C) Images (fixed after 24 h) of HaCaT cells (green) co-cultured with Control, EphB2
505 or ERK1/2 siRNA transfected HT1080 cells (magenta). Scale Bar = 100 μ m.

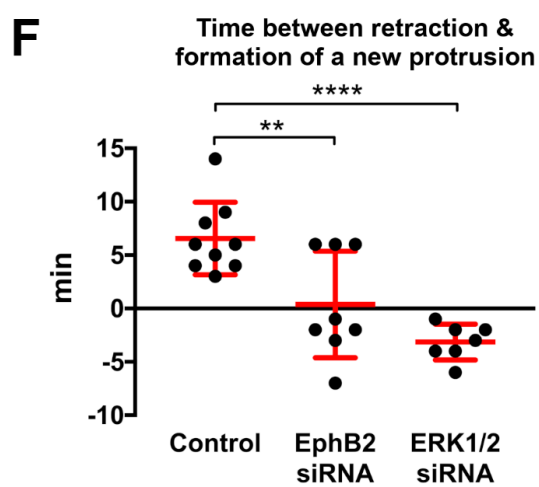
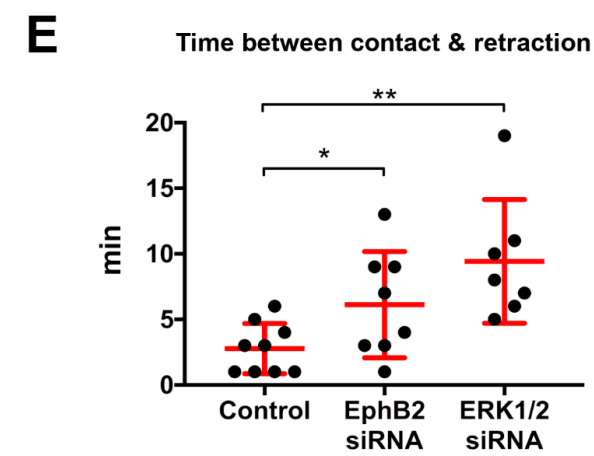
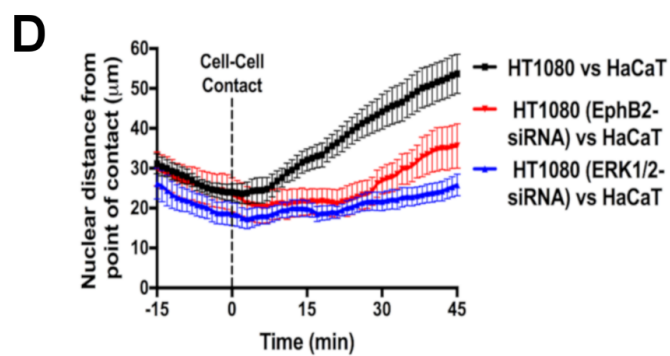
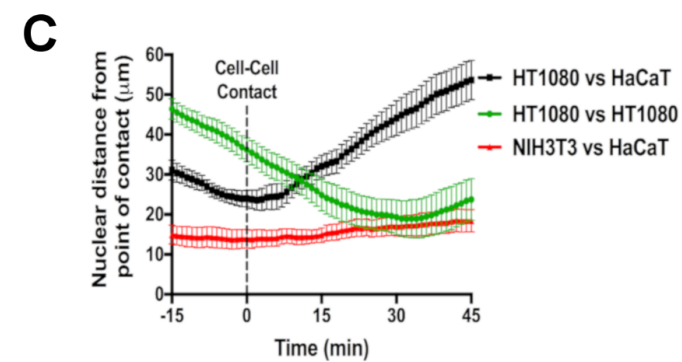
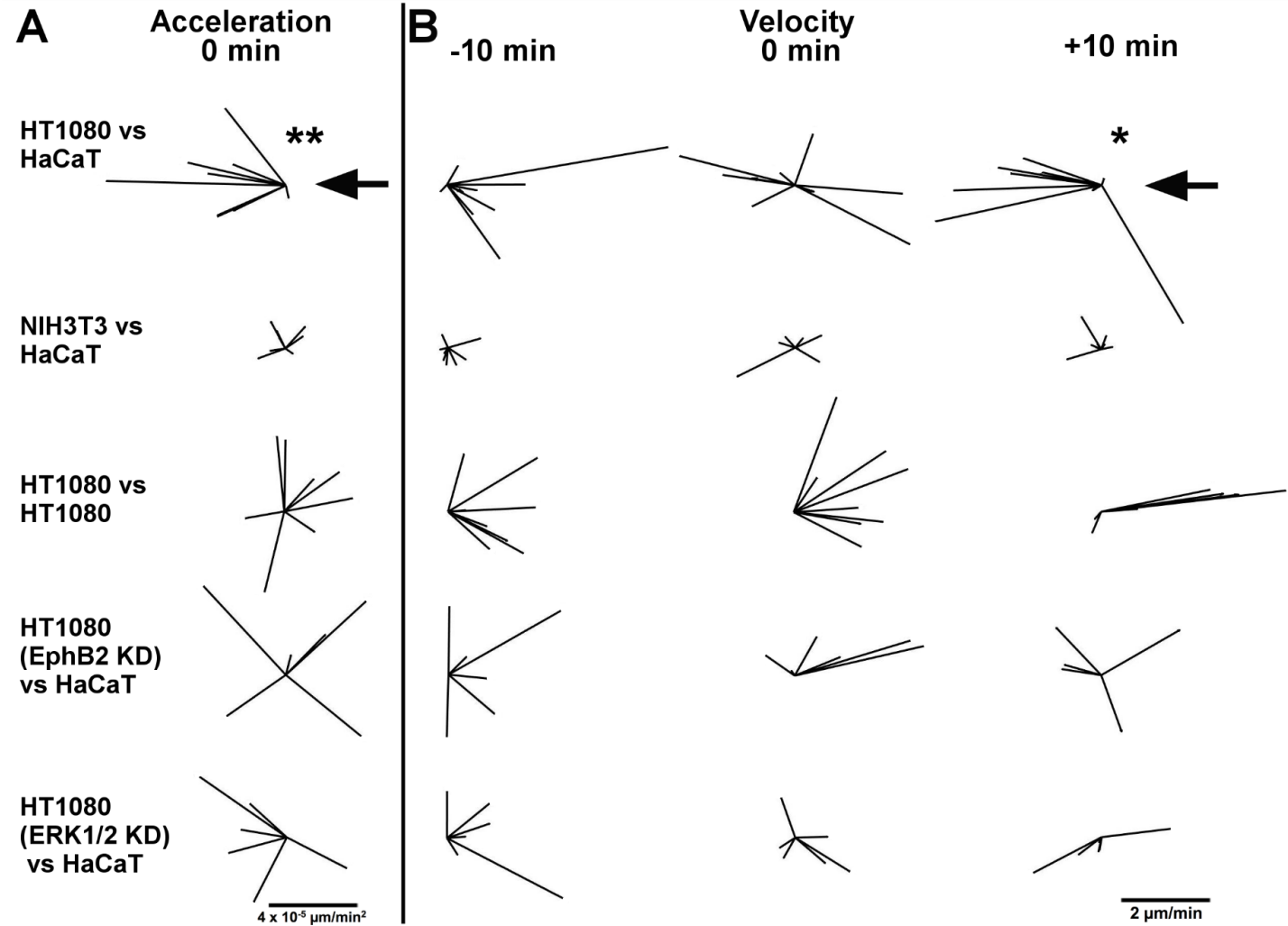
506 (D) Dispersion of HaCaT cells in 'C' quantified by measuring their distribution of
507 nearest-neighbour distances. (n = 3, error bars = SEM, **P < 0.01, *P < 0.05,
508 Student's t-test).

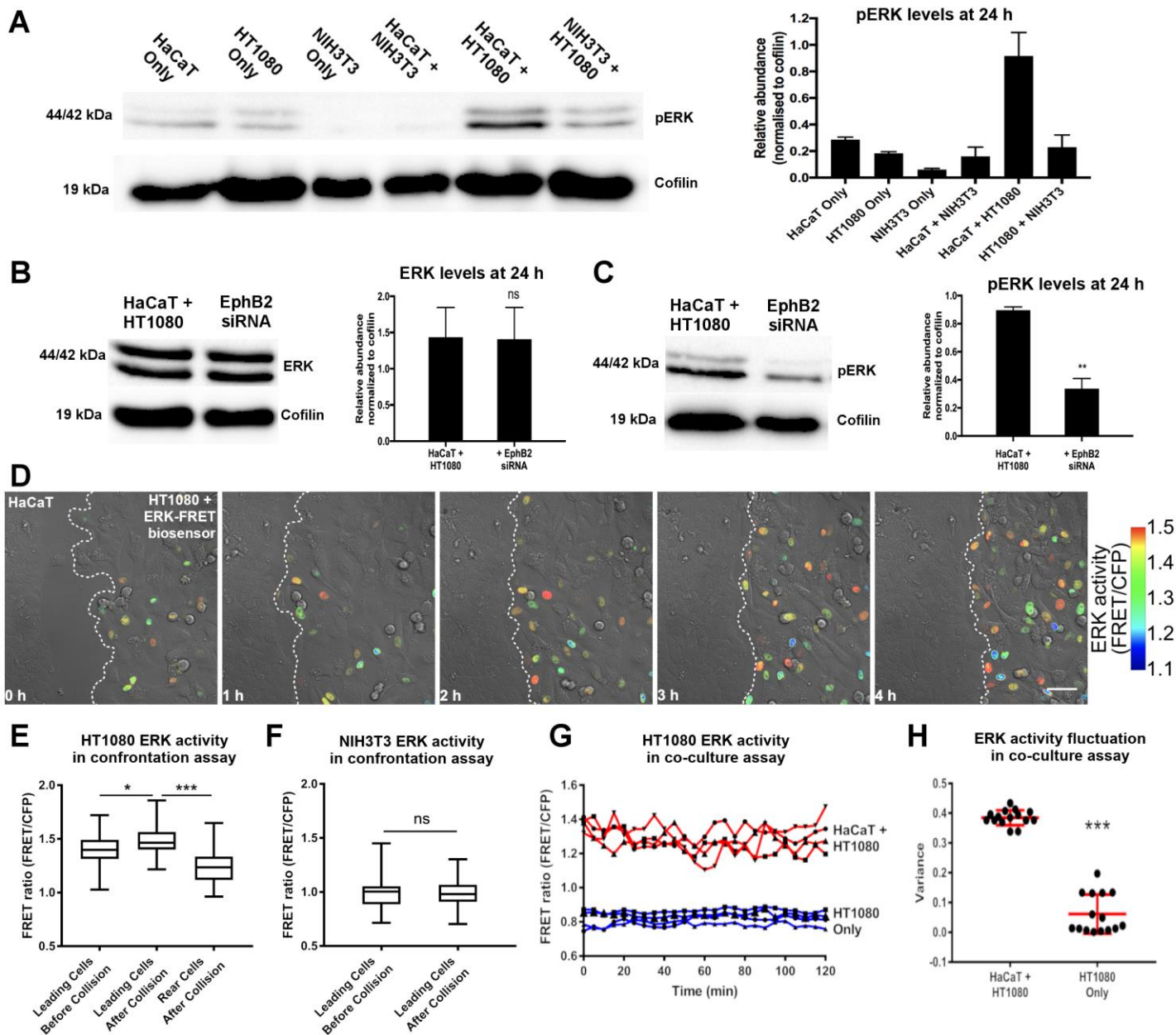
509 (E) Long term culture of HaCaT cells (green) alone or co-cultured with NIH3T3 or
510 HT1080 cells (unlabeled). Scale bar = 100 μ m.

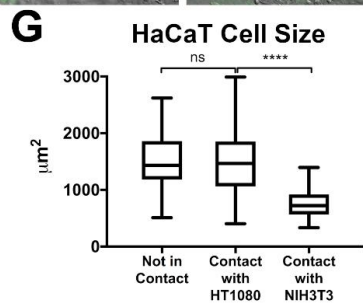
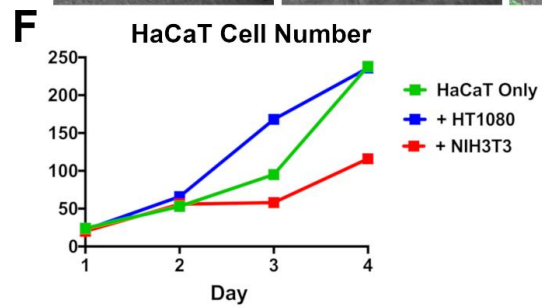
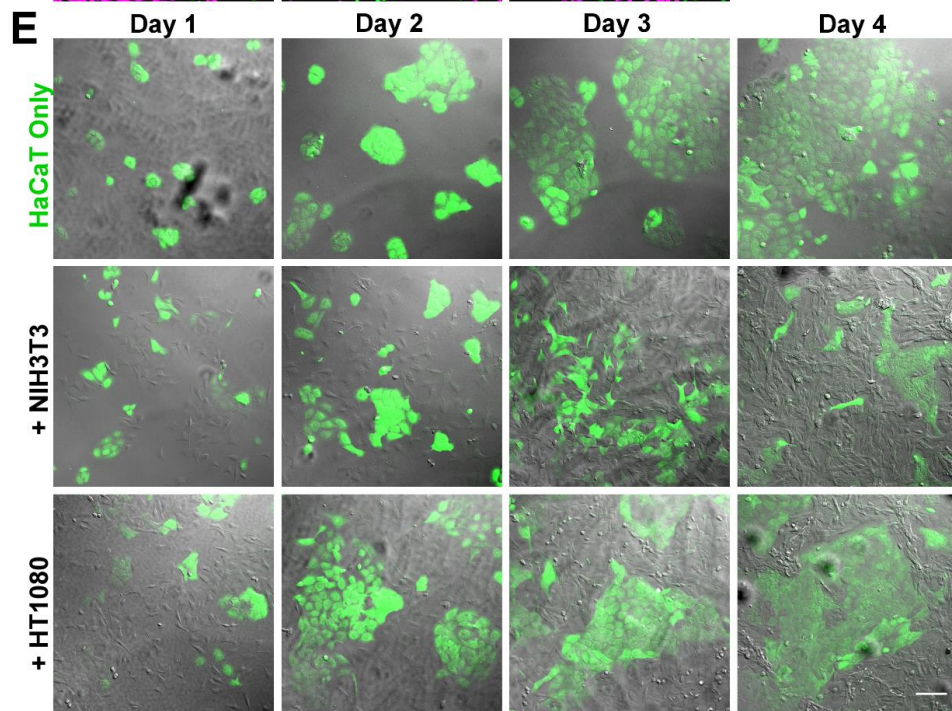
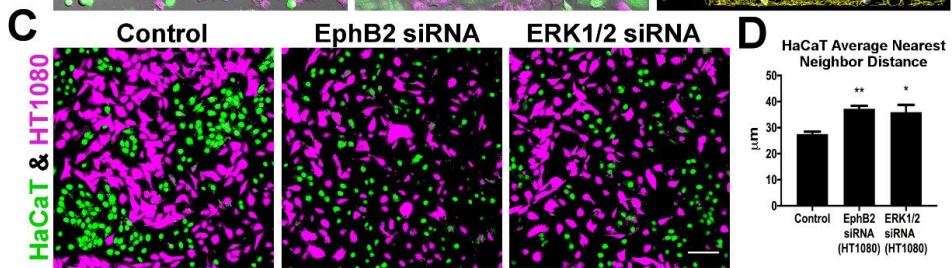
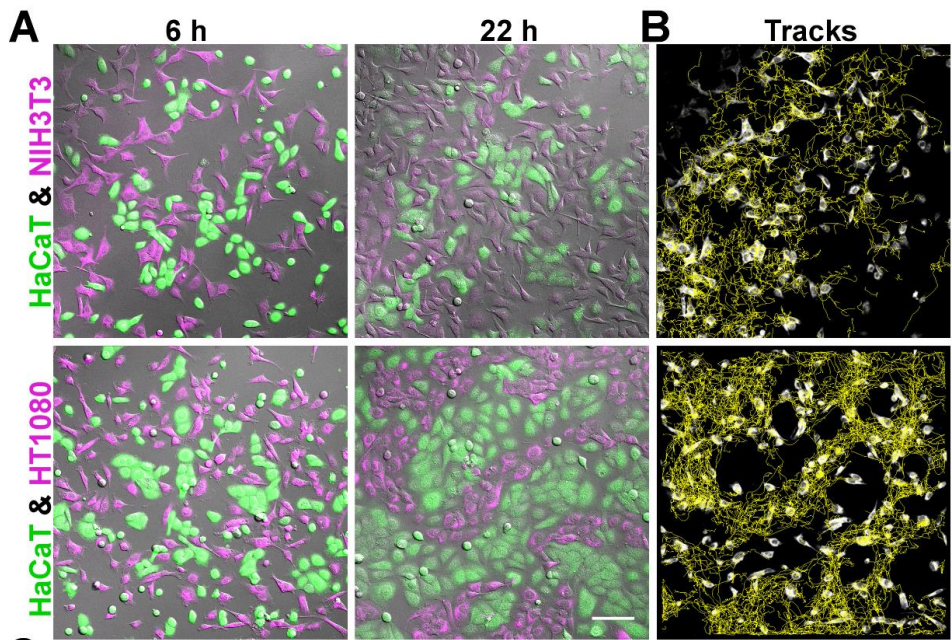
511 (F) HaCaT cell-number when grown in isolation or co-cultured showing reduced
512 HaCaT proliferation when co-cultured with NIH3T3 cells but not HT1080 cells.

513 (G) Size of individual HaCaT cells showing reduced spreading when contacting
514 NIH3T3 cells but not HT1080 cells. (****P < 0.0001, ns = not statistically significant,
515 Mann-Whitney test, n \geq 69 cells per condition).









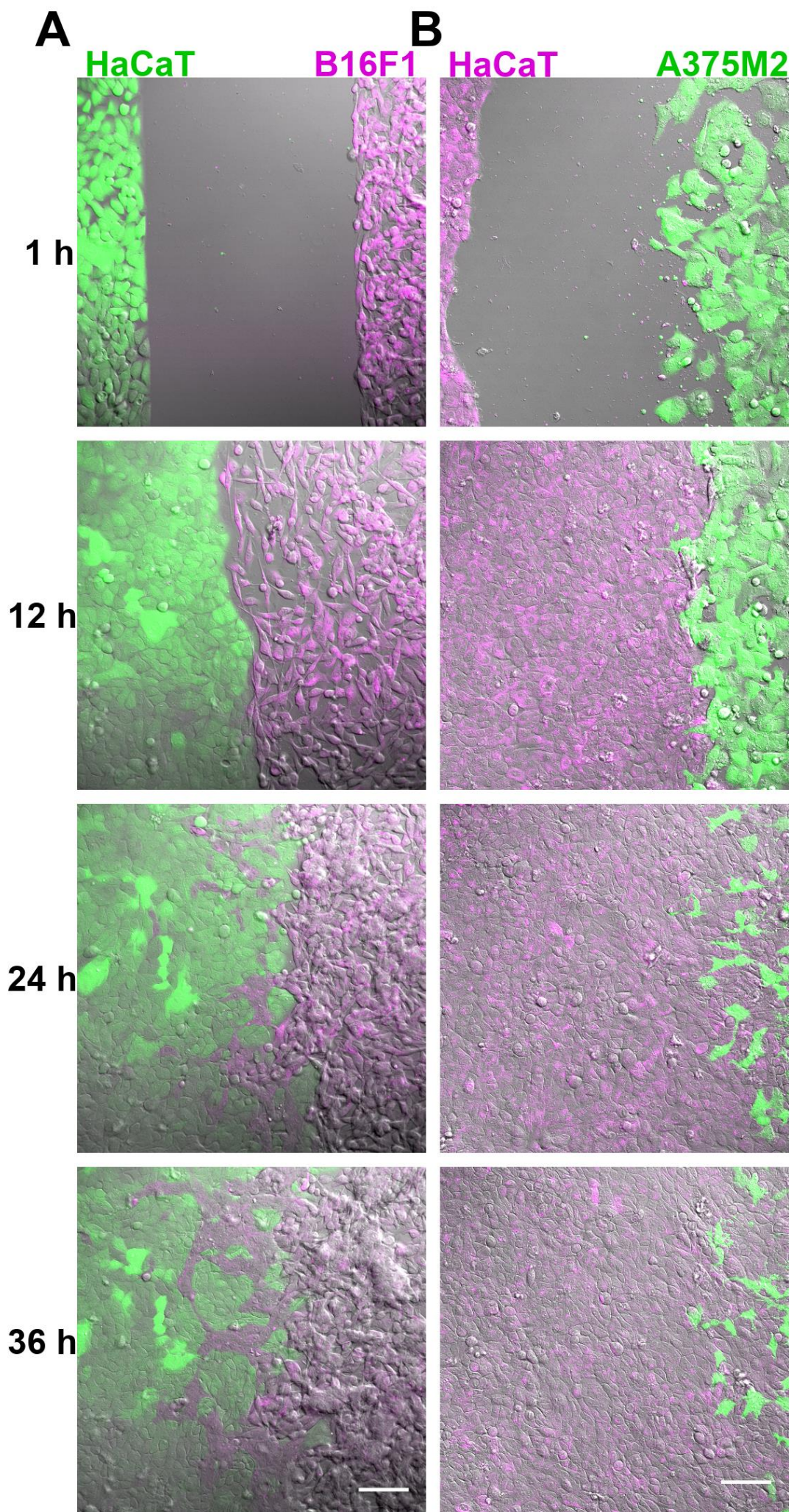


Figure S1.

(A) Confrontation assay between HaCaT human keratinocytes (green) and B16F1 mouse melanoma cells (magenta).

(B) Confrontation assay between HaCaT human keratinocytes (magenta) and A375M2 human melanoma cells (green).

Scale bars = 100 μ m.

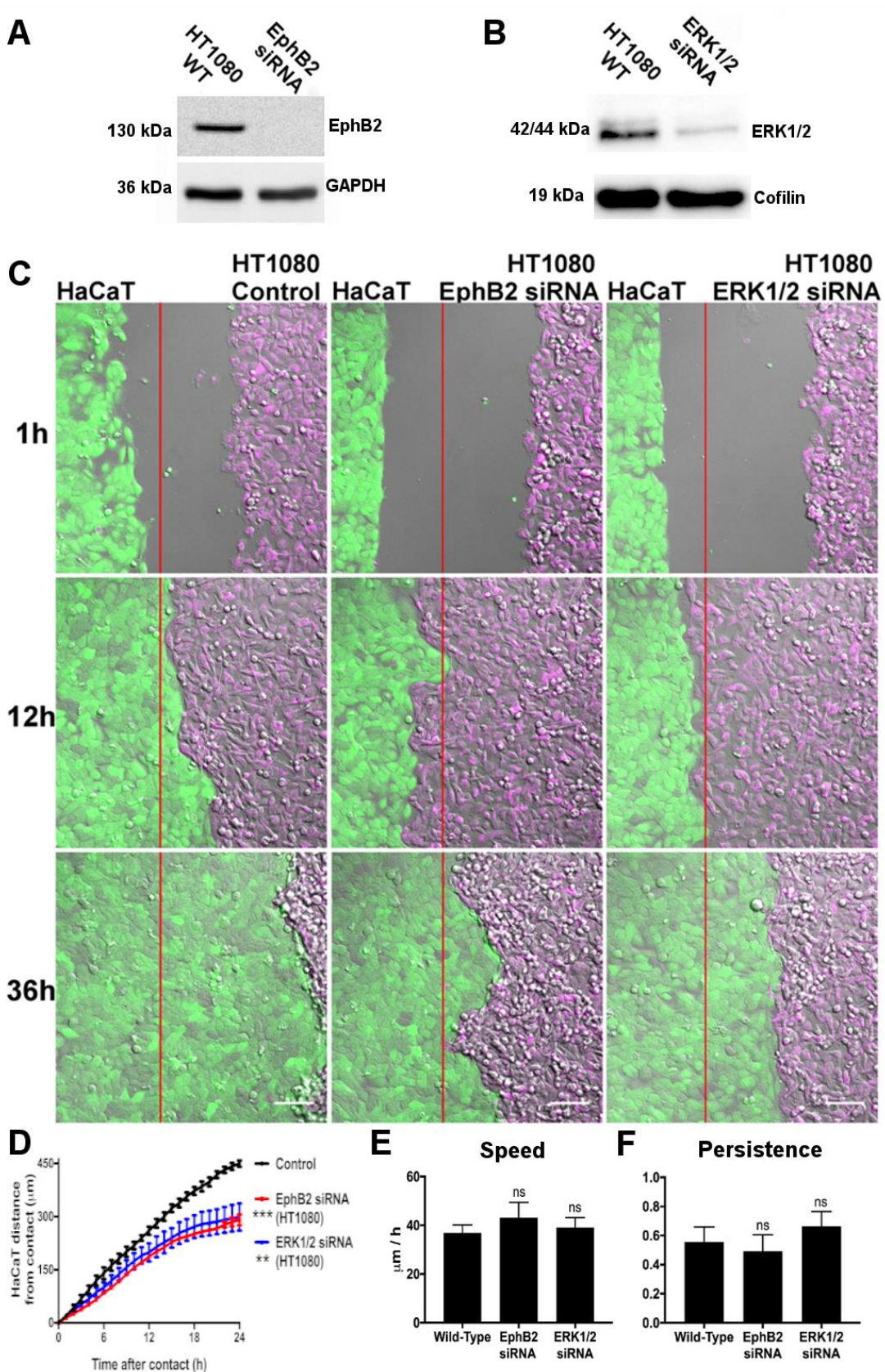


Figure S2.

- (A) Western blot confirming knockdown of EphB2 protein in HT1080 cells 48 h post-transfection with siRNA compared with non-transfected cells (WT = Wild Type).
- (B) Western blot confirming knockdown of ERK1/2 protein in HT1080 cells 48 h post-transfection with siRNA compared with non-transfected cells (WT = Wild Type).
- (C) Screenshots from a confrontation assay in which HaCaT cells (green) are allowed to collide with either Control, EphB2 or ERK1/2 siRNA transfected HT1080 cells (magenta). Red line indicates position of contact. Scale bars = 100 μm.
- (D) Displacement of HaCaT leading-edge after collision with HT1080 cells (Control, EphB2 or ERK1/2 siRNA) in the confrontation assay. (n = 3, error bars = SEM, ***P < 0.001, **P < 0.01, Friedman test).
- (E) Speed of non-colliding HT1080 cells transfected with either EphB2 or ERK1/2 siRNA compared with non-transfected (wild-type). (n = 10 cells, error bars = SEM, ns = not statistically significant, Student's t-test).
- (F) Persistence of non-colliding HT1080 cells transfected with either EphB2 or ERK1/2 siRNA compared with non-transfected (wild-type). (n = 10 cells, error bars = SEM, ns = not statistically significant, Student's t-test).

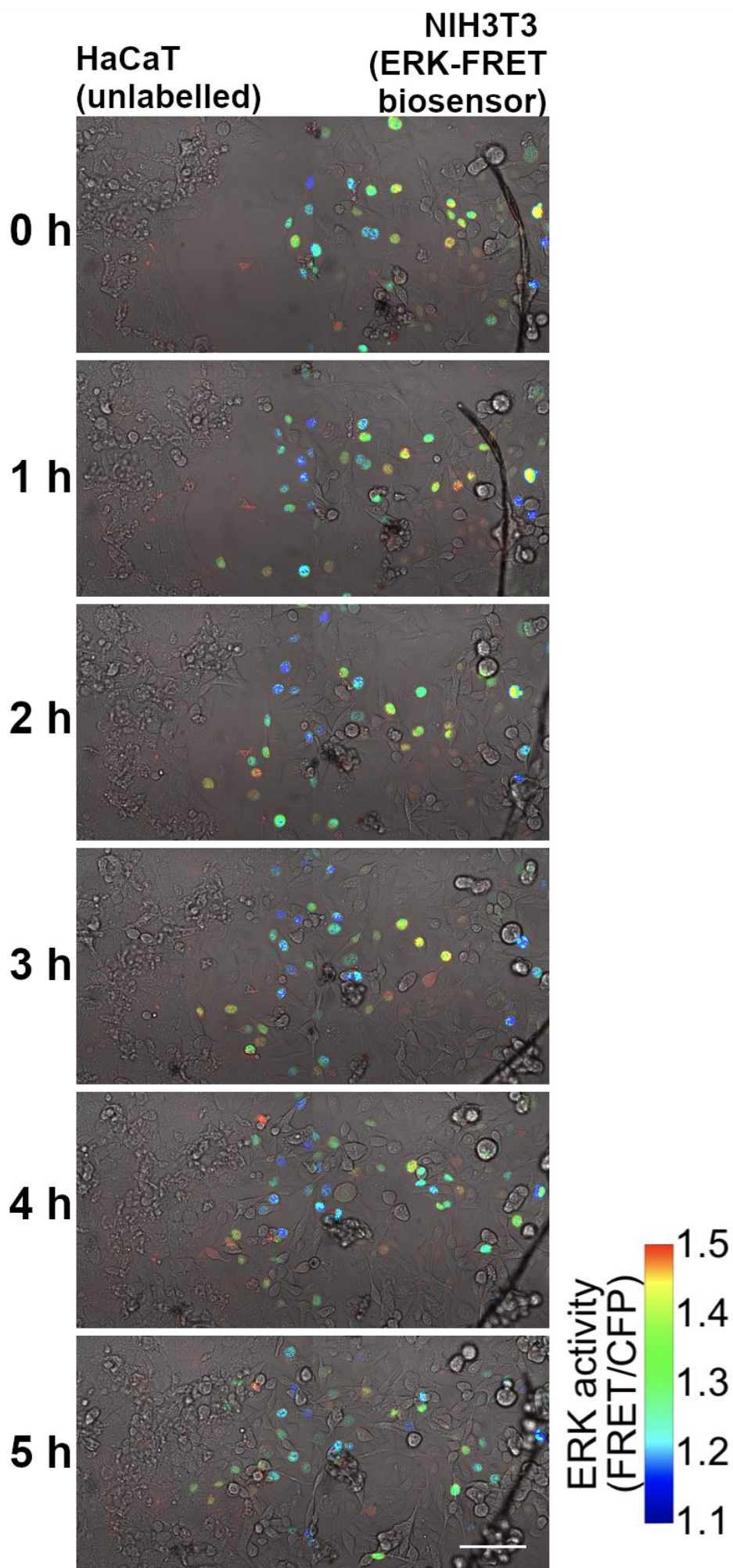


Figure S3. Confrontation assay between HaCaT cells (unlabelled) and NIH3T3 cells expressing the ERK FRET-biosensor. Scale bar = 100 μ m.

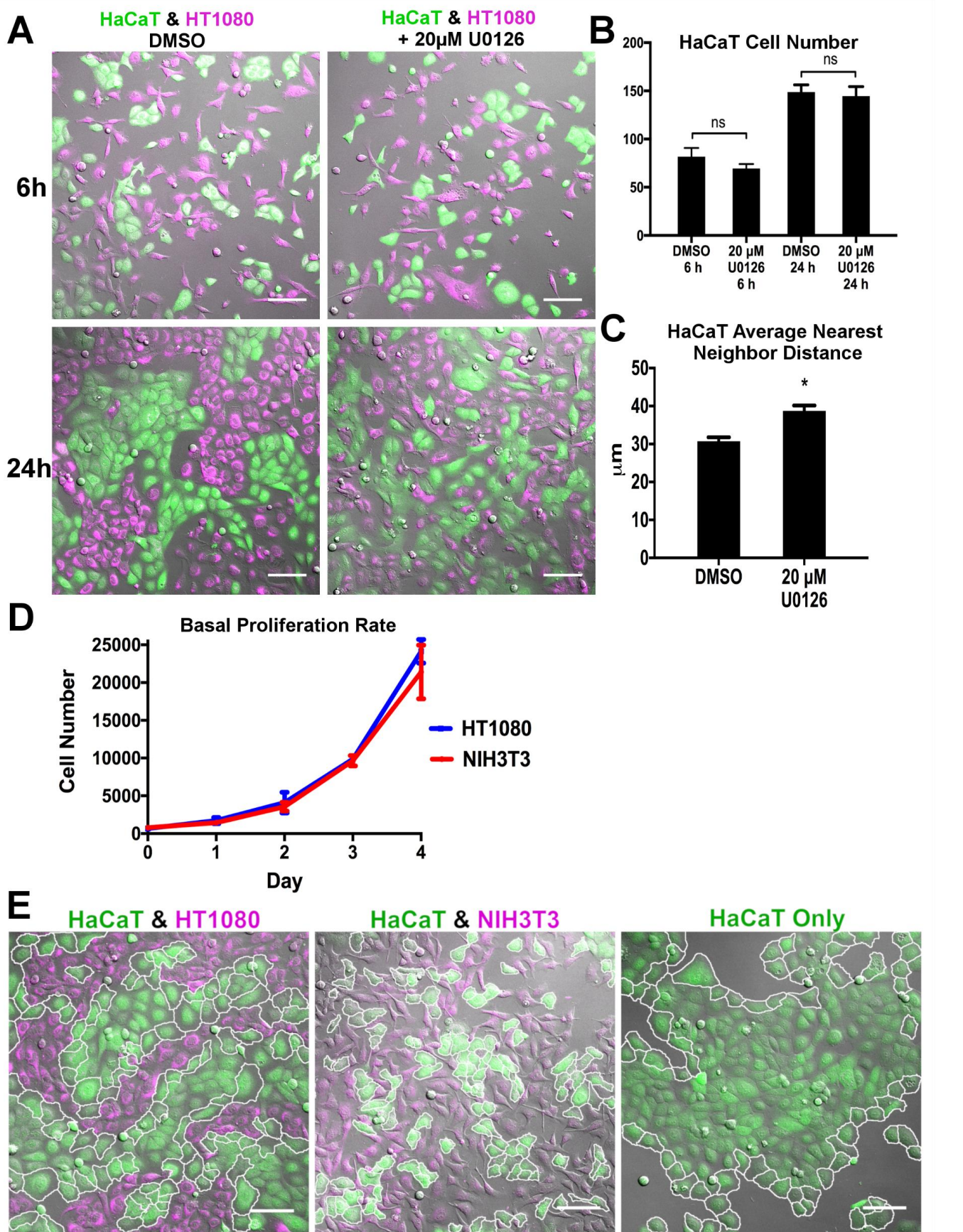


Figure S4.

- (A) Images of co-cultures of epithelial cells (HaCaT, green) with fibrosarcoma cells (HT1080, magenta) comparing DMSO vehicle control with 20 μ M U0126 treatment to inhibit ERK signalling.
- (B) Quantification of HaCaT cell numbers at 6 and 24 h to demonstrate that U0126 does not selectively impact the growth rate of HaCaT cells. (n = 3, error bars = SEM, ns = not statistically significant, Student's t-test).
- (C) The dispersion of HaCaT cells at 24 h quantified by measuring their distribution of nearest neighbor distances. An increase in HaCaT dispersion represents a reduction in their segregation from HT1080 cells. (n = 3, error bars = SEM, *P < 0.05, Student's t-test).
- (D) Basal proliferation rates of NIH3T3 and HT1080 cells (n = 3, error bars = mean \pm SD).
- (E) Screenshots showing the extent of spreading (quantified in Fig. 4G) of epithelial cells (outlined in white) when contacting HT1080 cells (left), NIH3T3 cells (middle), and when not in contact with either mesenchymal cell population (cultured alone, right).

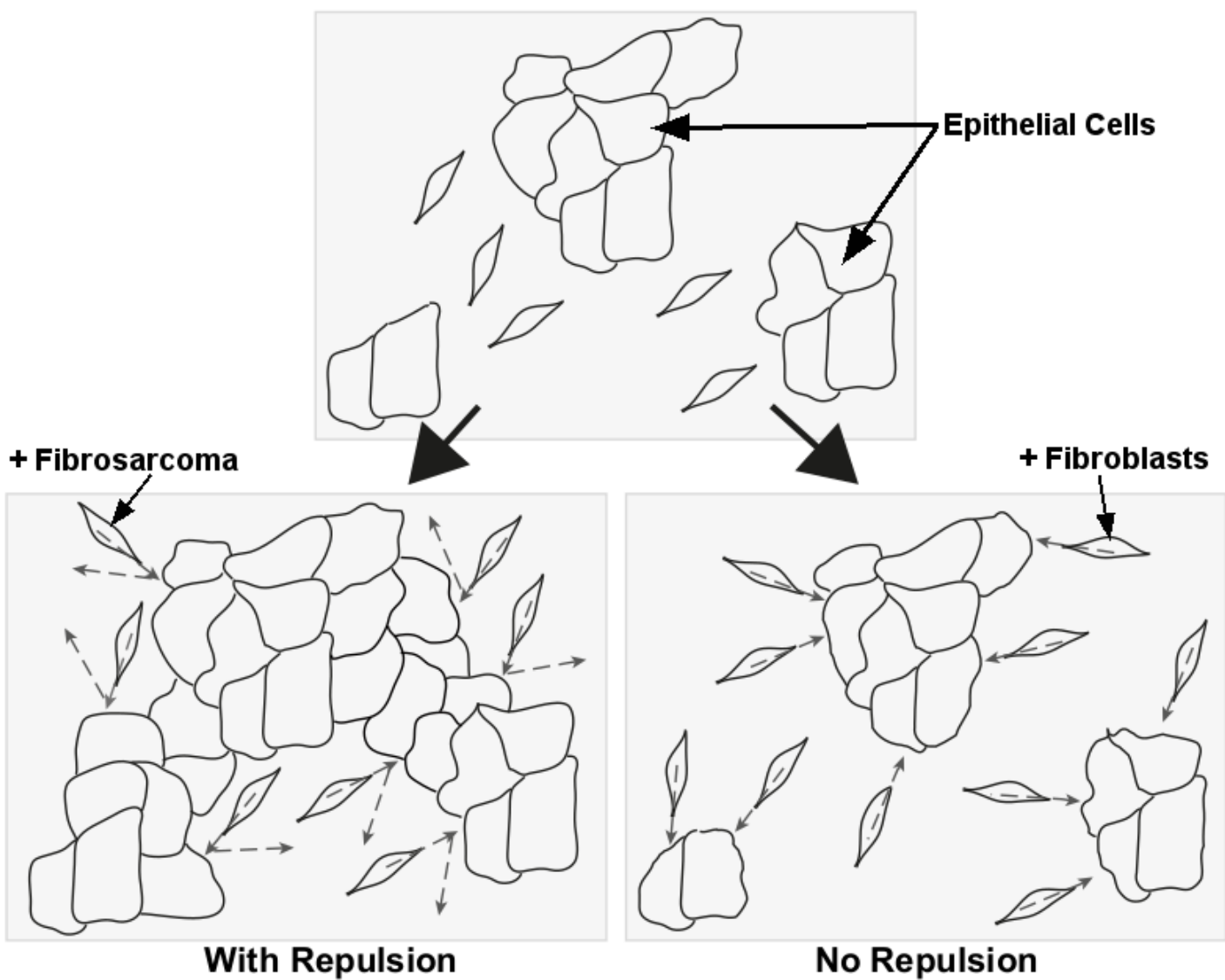


Figure S5. Schematic depicting our model of cell-sorting whereby a mesenchymal cell-type (fibrosarcoma, left) can rapidly and almost completely segregate from an epithelial population. We hypothesise that the strong heterotypic repulsion between fibrosarcoma and epithelial cells allows the epithelial cells to spread. Furthermore, there appears to be an aspect of fibrosarcoma CIL relieving contact inhibition of proliferation of epithelial cells, allowing epithelial colonies to proliferate and merge. In the fibroblast-epithelial combination (right), the epithelial cells are inhibited in their ability to spread due to a lack of heterotypic repulsion, which would enhance the spatial constraint on the epithelial colonies leading to their reduced proliferation. In this case the lack of repulsive CIL prevents the epithelial colonies from growing enough to merge with neighbouring colonies and thus separate from the fibroblast population.

Supplementary Movie Legends

Movie 1.

Confrontation assays between HaCaT epithelial cells (green) and NIH3T3 fibroblasts or HT1080 fibrosarcoma cells (magenta). 1h frames. Scale bar = 100 μm .

Movie 2.

Confrontation assays between:

HaCaT (human keratinocyte, green) vs B16F1 (mouse melanoma, magenta).

HaCaT (human keratinocyte, magenta) vs A375M2 (human melanoma, green).

1 h frames. Scale bar = 100 μm .

Movie 3.

Particle Image Velocimetry (PIV) heat-map of the HaCaT and HT1080 interaction showing global increase in HaCaT cell speed after colliding with HT1080 cells. Blue to red represents a shift from low to high instantaneous velocity. 1 h frames.

Movie 4.

Individual HT1080 fibrosarcoma cells (Control, EphB2 or ERK1/2 siRNA transfected) colliding with HaCaT epithelial cells or homotypic collisions between HT1080 cells. Red lines represent manual tracking used for the kinematics analysis. 10 sec frames. Scale Bar = 20 μm .

Movie 5.

Confrontation assay between HaCaT cells (unlabelled) and HT1080 cells expressing the ERK FRET-biosensor. Blue to red represents an increase in ERK activity (FRET/CFP).

5 min frames. Scale bar = 50 μm .

Movie 6.

(Top) Co-culture assay whereby HaCaT cells (green) are co-cultured with either NIH3T3 cells (left, magenta) or HT1080 cells (right, magenta). 10 min frames. Scale bar = 100 μm .

(Bottom) Tracks of NIH3T3 fibroblasts (left) and HT1080 fibrosarcoma cells (right) from the movies above. Tracks shift blue to red throughout movie to demonstrate that, in the HT1080 case (bottom right), cells become segregated from HaCaT cells (not labelled) over time.